processes

MDPI

Article

Study on the Influence Mechanism of Air Leakage on Gas Extraction Effect—A Numerical Case Study of the Coal Mine Site in Anhui

Han Gao [1,2], Feng Du [2,*], Xiaoyu Cheng [1], Jinjie Zhang [3] and Aitao Zhou [2]

[1] China Coal Energy Research Institute Co., Ltd., Xi'an 710054, China; gaohan1986@126.com (H.G.); chengxiaoyu89@126.com (X.C.)
[2] School of Emergency Management and Safety Engineering, China University of Mining and Technology (Beijing), Beijing 100083, China; cumtbzat@126.com
[3] China Coal Xinji Liuzhuang Mining Co., Ltd., Fuyang 236200, China; 18755435573@163.com
* Correspondence: fdu@cumtb.edu.cn

Abstract: Air leakage in mine gas drainage drilling is a critical factor that affects gas extraction efficiency. It leads to a rapid decline in gas concentration, resulting in lower extraction efficiency and potential secondary disasters. To address this issue, a fully coupled gas–air mixed flow model is established in this study. The model examines the effects of extraction time, different negative pressures, and gas leakage on gas concentration. Additionally, it reveals the mechanism of air leakage around gas drainage boreholes. The simulation data are then compared with field gas drainage monitoring data to verify the reliability of the model. This verification serves as a basis for extraction regulation and control. The results demonstrate that during the later stages of extraction, the negative pressure decreases, causing a decline in gas concentration. Moreover, higher negative pressure leads to increased air inflow into the borehole, thereby reducing gas concentration. Consequently, selecting an appropriate negative pressure is crucial to improve pumping efficiency. The research findings hold significant guidance in achieving efficient gas mining.

Keywords: gas extraction; air leakage; permeability; diffusion-seepage

Citation: Gao, H.; Du, F.; Cheng, X.; Zhang, J.; Zhou, A. Study on the Influence Mechanism of Air Leakage on Gas Extraction Effect—A Numerical Case Study of the Coal Mine Site in Anhui. *Processes* **2023**, *11*, 2161. https://doi.org/10.3390/pr11072161

Academic Editor: Guining Lu

Received: 15 June 2023
Revised: 17 July 2023
Accepted: 18 July 2023
Published: 19 July 2023

1. Introduction

In recent years, new energy sources have experienced rapid development. However, coal is expected to remain the primary energy source in China for the foreseeable future. In order to ensure resource utilization and minimize secondary disasters, the co-mining of coal and gas has gained significance [1–4]. First and foremost, it is crucial to prioritize the safety of coal mining operations. The mining process is prone to various dynamic disasters, with gas-related incidents being particularly common. The quantity and efficiency of gas extraction from coal seams directly impact the safety of coal mines. One major challenge in mine gas drainage is the rapid attenuation of gas concentration. This hampers effective gas utilization, leading to environmental pollution and the risk of gas explosions and other hazards [5–8]. Therefore, implementing effective gas pre-drainage measures holds immense importance in ensuring coal mine safety and optimizing gas resource utilization.

The coal seam gas drainage boreholes are typically categorized into main pipes and branch pipes. Multiple boreholes are interconnected and eventually merged into the main extraction pipeline [9,10]. Currently, it is a common practice to arrange these pipes from the surface to the underground coal seam for gas pre-drainage [11–13]. However, the majority of coal seams in our country have low permeability, resulting in poor gas drainage effectiveness. Additionally, there is a significant issue of gas leakage due to limitations in sealing technology. Although sealing technology has witnessed advancements in recent years, these challenges have not been fundamentally resolved. As extraction progresses

into the middle and later stages, there is a noticeable decline in gas concentration, which attenuates rapidly [14]. This is attributed to the development of coal and rock mass cracks caused by mining disturbances. Furthermore, the overall gas concentration is further reduced due to the decrease in the total gas volume. If the gas concentration in the drainage pipeline falls within the explosion limit, it poses a threat to the safe production of the coal mine. Simultaneously, the discharge of gas with lower concentrations into the atmosphere can have adverse environmental impacts.

Coal is considered a dual-porosity medium [15], where gas exists both in the fractures of coal in a free state and in the matrix pores in an adsorbed state, with a significant proportion being adsorbed gas. During the process of gas extraction from coal seams, the gas typically undergoes three processes: desorption, diffusion, and seepage [16]. To understand the cross-coupling mechanism of various physical fields during coalbed methane drainage, extensive research has been conducted by scholars. Liu et al. [17] conducted a comprehensive analysis of the research progress on multiphysics coupling processes in coalbed methane mining. They concluded that the complex interaction between stress, chemical fields, mining processes, and geological fluid injection significantly impacts the geomechanical characteristics of coal. Liang et al. [18] constructed a multi-field coupling model incorporating stress–diffusion–seepage to investigate the gas flow behavior around drilled holes during coal seam extraction, focusing on the optimal spacing of boreholes for gas drainage. Wu et al. [19] developed a multi-field coupling model considering coal deformation, gas adsorption, diffusion, seepage, and humidity effects to study the evolution of flow fields and competitive gas adsorption behavior during CO_2 geological storage and enhanced coalbed methane mining. Zhai et al. [20] integrated coal gas permeability with mechanical properties and gas adsorption/desorption, establishing a mathematical model to analyze transient stresses and dynamic leakage flow fields around extraction boreholes. Cheng et al. [21] established a gas–solid coupling model considering fracture gas seepage, permeability evolution, and coal deformation to analyze the influence of diffusion and seepage on gas transport and investigate the mechanism of negative pressure in the gas extraction process. Hao et al. [22] developed a fluid–structure interaction model that accounted for coal creep effects to determine the effective radius of boreholes at different burial depths. Wang et al. [23] established a dynamic permeability change model of coal seams considering effective stress, gas desorption, and coal matrix shrinkage effects, simulating the penetration changes based on different coal seam gas pressures. Wang et al. [24] derived a formula representing the gas flow resistance of coal seams using the matchstick model combined with Darcy's law and the Hagen–Poiseuille equation, illustrating the influence of fracture curvature, gas pressure, and effective stress on gas flow resistance. Zang et al. [25] derived an orthotropic permeability evolution equation considering effective stress and expansion stress based on coal body mechanical properties and initial porosity anisotropy. Liu et al. [26] simulated gas pressure distribution under different adsorption times and investigated the influence of the Klinkenberg effect on gas extraction. Liu et al. [27] applied a diffusion–seepage gas migration model to simulate the change in matrix pore and fracture gas pressure over time under dynamic changes in the diffusion coefficient. Zhang et al. [28] studied the influence mechanism of negative pressure on drainage effectiveness, simulated the change in gas concentration under different negative pressures and sealing parameters, and provided guidance for improving gas drainage drilling hole sealing technology. Liu et al. [29] conducted a systematic analysis of the multi-field coupling process and various factors affecting gas drainage in deep mines, offering guidance for enhancing gas drainage efficiency. Although extensive studies have been conducted on the multi-field coupling of coal-gas systems, research on underground gas extraction processes in coal mines has primarily focused on single-component gas flow, with limited exploration of multi-field coupling in air-gas binary gas systems involving borehole air leakage processes. The lack of systematic research and a comprehensive theoretical basis presents certain challenges.

In order to tackle these challenges, this paper introduces a multi-field coupling model that focuses on the "air–gas" binary gas flow during borehole gas extraction. The model takes into account various factors, including coal matrix deformation, pore gas diffusion, fracture gas seepage, and the coupling effect of air leakage. By considering these interconnected aspects, the model provides a comprehensive understanding of the gas extraction process. The research findings from this multi-field coupling model hold great significance in terms of improving the efficiency of gas utilization and preventing and mitigating disasters. This approach allows for a better optimization of gas extraction processes and enhances the overall safety of mining operations.

2. Theoretical Model Construction

During the gas pre-drainage process from boreholes in this coal seam, it is commonly observed that there is initially a high gas concentration and flow rate. However, as the extraction time progresses, there is a varying degree of decrease in gas concentration and flow. This decline can be attributed to changes in the number, spacing, and aperture of cracks influenced by mining-induced stress and gas pressure, indicating the dynamic development of the fracture state. Figure 1 illustrates the pathways created by the development and penetration of the fracture network, allowing ventilation air from the roadway to enter the extraction hole. The pore structure of the coal is depicted in Figure 2. Identifying the precise locations of high permeability areas for air leakage around the borehole is crucial for effective sealing and plugging of fracture channels. To accomplish this, a double-hole-mixed gas seepage coupling model was established to study the permeability evolution in different coal areas surrounding gas drainage boreholes and identify the areas with high permeability for air leakage.

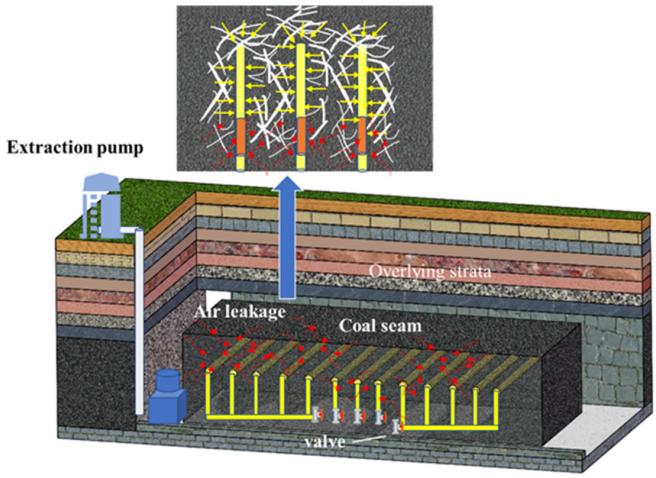

Figure 1. Schematic diagram of the on-site drilling layout.

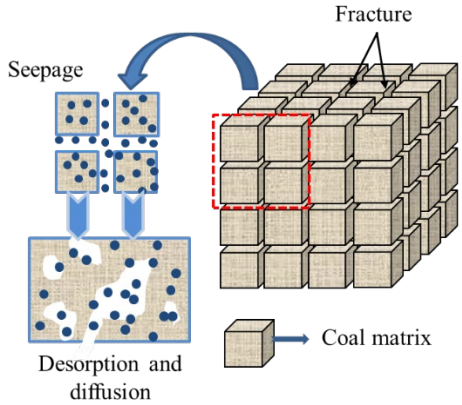

Figure 2. Schematic diagram of ideal coal body composed of coal matrix and cracks.

This model makes the following assumptions:

(1) The pressure generated by air in the fractures is considerably lower than the gas pressure within the pores of the coal matrix. Hence, the adsorption and migration of air within the coal matrix are not considered. Air is assumed to flow solely within the coal fissures.
(2) Gas behavior follows the principles of Fick's diffusion and Darcy's seepage during its flow.
(3) The migration of gas and air within the coal is assumed to be isothermal, neglecting any heat exchange.
(4) The seepage of gas and air within the fracture space is treated as independent processes. The deformation and permeability evolution of coal are mainly influenced by the superposition of gas pressure and air pressure.

2.1. Mechanical Constitutive Relation of Coal

Under the action of free gas and adsorbed gas, the deformation and mechanical properties of gas-bearing coal change, which makes the stress field change accordingly.

Coal is a double-pore structure; the relationship between surface stress and bulk stress can be expressed as outlined in reference [30]:

$$\sigma_{ij,j} + F_i = 0, \tag{1}$$

where $\sigma_{ij,j}$ is the stress tensor along j direction, MPa; and F_i is the volume force in the direction of i, MPa.

The coal cracks considering air leakage contain gas–air two-component gas. Therefore, the gas pressure in coal fissures and the gas pressure in coal matrix pores can be expressed as follows:

$$p_f = p_{fa} + p_{fg}, \tag{2}$$

where p_f is the total gas pressure in coal fissures, MPa; p_{fa} is the air pressure in coal fissures, MPa; and p_{fg} is the gas pressure in coal fissures, MPa.

$$p_m = p_{mg}, \tag{3}$$

where p_m is the total pressure of gas in coal matrix, Mpa; and p_{mg} is the gas pressure in coal matrix, MPa.

According to the effective stress principle put forward by Terzaghi, combined with the continuous modification of the effectiveness of rock mass media, the effective stress of coal is expressed by Formula (4):

$$\begin{cases} \sigma_{ij} = {\sigma_{ij}}^e - \left[\alpha_f\left(p_{fa} + p_{fg}\right) + \alpha_m p_{mg}\right]\delta_{ij} \\ \alpha_f = 1 - \frac{K}{K_m} \\ \alpha_m = \frac{K}{K_m} - \frac{K}{K_s} \\ K_m = \frac{E_m}{3(1-2v)} \\ K_s = \frac{E_m}{3(1-2v)-9\phi_m(1-v)/2} \end{cases}, \tag{4}$$

where σ_{ij} is the normal stress acting on coal, MPa; ${\sigma_{ij}}^e$ is the effective stress on coal, MPa; α_f is the effective stress coefficient of coal body crack; α_m is the effective stress coefficient of coal matrix; δ_{ij} is the Kronecker function; K is the coal bulk modulus, MPa; K_m is the coal matrix bulk modulus, MPa; K_s is the coal solid skeleton bulk modulus, MPa; E is the young 's modulus of coal, MPa; E_m is the young's modulus of coal matrix, MPa; ϕ_m is the porosity of coal matrix; and v is the Poisson's ratio of coal.

The constitutive relation of stress and strain of gas-bearing coal is expressed as follows [31]:

$$\sigma_{ij}{}^{e} = 2G\varepsilon_{ij} + \frac{2G}{1-v}\varepsilon_v\delta_{ij} - K\varepsilon_b{}^{s}\delta_{ij}, \tag{5}$$

where G is the shear modulus of coal, MPa, $G = \frac{E}{2(1+v)}$; ε_{ij} is the strain tensor of coal mass; ε_v is the volumetric strain of coal; and $\varepsilon_b{}^{s}$ is the volumetric strain caused by coal adsorption.

Among them is the following:

$$\varepsilon_b{}^{s} = \frac{\varepsilon_{b\max}{}^{s} p_m}{p_m + p_L}, \tag{6}$$

where $\varepsilon_{b\max}{}^{s}$ is the maximum strain produced by adsorbing gas; and p_L is the type Langmuir adsorption strain pressure.

Displacement and strain can be expressed by Equation (7):

$$\varepsilon_{ij} = \frac{1}{2}(u_{i,j} + u_{j,i}), \tag{7}$$

where ε_{ij} is the strain component; and $u_{i,j}$, $u_{j,i}$ are the displacement component.

The following Equation (8) is obtained:

$$Gu_{i,ij} + \frac{G}{1-2v}u_{j,ji} - \alpha_f\left(p_{fg,i} + p_{fa,i}\right) - \alpha_m p_{m,i} - K\varepsilon^{s}{}_{b,i}\delta_{ij} + F_i = 0. \tag{8}$$

The failure behavior of coal can be expressed by formula [32]:

$$F = \frac{\sin\varphi}{\sqrt{3}\sqrt{3+\sin^2\varphi}}I_1 + \frac{3C\cos\varphi}{\sqrt{3}\sqrt{3+\sin^2\varphi}} - \sqrt{J_2}, \tag{9}$$

where I_1 is the first invariant of the stress tensor, $I_1 = \sigma_1 + \sigma_2 + \sigma_3$; I_2 is the second invariant of the stress tensor, $I_2 = \sigma_1\sigma_2 + \sigma_2\sigma_3 + \sigma_3\sigma_1$; J_2 is the second invariant of stress deviation, $J_2 = \frac{1}{3}{I_1}^2 - I_2$; φ is the internal friction angle; and C is the cohesive force.

2.2. Gas Migration Model

Considering air leakage, a diffusion-seepage model is established.

2.2.1. Subsubsection

In a coal body structure with a double pore system, the gas components in the coal matrix primarily consist of adsorbed gas within the matrix and free gas within the matrix pores. Therefore, the total gas quantity per unit volume of the coal matrix can be expressed as stated in reference [33]:

$$m_m = \frac{V_L p_m}{p_m + P_L} \cdot \frac{\rho_c M_C}{V_m} + \frac{\phi_m p_m M_g}{RT}, \tag{10}$$

where m_m is the total amount of gas per unit volume of coal matrix, kg/m^3; p_m is the total pressure of gas in coal matrix, Mpa; V_m is the coal matrix volume, cm^3; M_c is the molar mass of methane under the standard condition, g/mol; V_L is the Langmuir volume, m^3/kg; P_L is the Langmuir pressure, MPa; ϕ_m is the Coal matrix porosity; ρ_c is the coal density, kg/m^3; R is the gas constant; T is the gas temperature, K; M_g is the molar mass of gas, the equivalent of gas in this paper is methane, its value is 16 g/mol.

In the absence of mining disturbances, the gas pressure within the original coal seam remains constant. However, the gas balance state within the coal matrix and fracture system undergoes changes due to gas drainage. During the operation of the extraction system, the gas flow velocity differs between the coal matrix and fracture system. The gas pressure within the fractures is relatively lower compared to the matrix. As a result, gas in the

fractures is replenished by the gas present in the coal matrix. This replenishment is driven by the difference in gas concentration. Therefore, the diffusion equation can be expressed as follows [34]:

$$Q_m = D\chi_s V_m\left(c_m - c_{fg}\right), \tag{11}$$

where Q_m is the diffusion source, kg/(m^3·s); D is the diffusivity, m^2/s; χ_s is the matrix shape factor, m^{-2}, $\chi_s = \frac{3\pi^2}{L^2}$; V_m is the coal matrix volume, cm^3; c_m is the gas concentration in coal matrix, kg/m^3, $c_m = \frac{M_g}{Z_m RT} p_m$; c_{fg} is the gas concentration in coal fissures, kg/m^3, $c_{fg} = \frac{M_g}{Z_{fg} RT} p_{fg}$; and L is the pore spacing, m.

Due to the shape factor being related to the adsorption time, the adsorption time τ is introduced as a parameter to characterize the diffusion behavior. It is numerically equal to the time it takes for the gas content in the coal matrix to be desorbed to 62.3% of the total. The matrix shape factor can be specifically expressed as follows [35]:

$$\tau = \frac{1}{D\chi_s}. \tag{12}$$

It can be expressed by mass conservation equation in the process of gas diffusion:

$$Q_m = -\frac{\partial m_m}{\partial t}. \tag{13}$$

By bringing Formulae (10) and (11) into Formula (13), you can obtain the following:

$$\frac{\partial p_m}{\partial t} = -\frac{V_m}{\tau \rho_c RT} \cdot \frac{\left(p_m - p_{fg}\right)}{\left(\frac{V_L p_L}{(p_m + P_L)^2} + \frac{\phi_m}{\rho_c p_0}\right)}. \tag{14}$$

2.2.2. Seepage Control Equation of Gas–Air Two-Component Gas in Fissures

The amount of gas in coal fissures per unit mass can be expressed as follows:

$$m_{fg} = \frac{\phi_f p_{fg} M_g}{RT} \tag{15}$$

$$m_{fa} = \frac{\phi_f p_{fa} M_a}{RT}, \tag{16}$$

where m_{fg} is the gas content in coal fissures per unit mass, m^3/kg; m_{fa} is the air content in coal fissures per unit mass, m^3/kg; and M_a is the molar mass of air, g/mol.

In the fracture system, the gas–air two-component gas flows under the action of the driving force caused by the gas concentration difference. There are as follows:

$$V_f = -\frac{k_f}{\mu}\nabla\left(p_{fg} + p_{fa}\right) \tag{17}$$

$$\mu = \frac{\mu_g}{1 + \frac{x_a}{x_g}\sqrt{\frac{M_a}{M_g}}} + \frac{\mu_a}{1 + \frac{x_g}{x_a}\sqrt{\frac{M_g}{M_a}}}, \tag{18}$$

where V_{fg} is the gas seepage rate in coal fissures, m/s; V_{fa} is the air seepage rate in coal fissures, m^3/kg; μ is the average dynamic viscosity of gas mixture in coal fissures, Pa·s; μ_g is the dynamic viscosity of gas, Pa·s; μ_a is the dynamic viscosity of air, Pa·s; x_g is the mole fraction of gas; and x_a is the mole fraction of gas.

Combined with the ideal state gas equation, the mole fraction of each component can be expressed as follows:

$$\begin{cases} x_g = \frac{n_g}{n_g+n_a} = \frac{p_{fg}}{p_{fg}+p_{fa}} \\ x_a = \frac{n_a}{n_a+n_g} = \frac{p_{fa}}{p_{fg}+p_{fa}} \end{cases}. \tag{19}$$

There are

$$\mu = \frac{\mu_g}{1+\frac{p_{fa}}{p_{fg}}\sqrt{\frac{M_a}{M_g}}} + \frac{\mu_a}{1+\frac{p_{fg}}{p_{fa}}\sqrt{\frac{M_g}{M_a}}}. \tag{20}$$

The gas flow equation of each component can be expressed as follows:

$$\begin{cases} \frac{\partial m_{fg}}{\partial t} = -\nabla\left(\rho_{fg}V_f\right) + \left(1-\phi_f\right)Q_m \\ \frac{\partial m_{fa}}{\partial t} = -\nabla\left(\rho_{fa}V_f\right) \end{cases}. \tag{21}$$

The Formulae (15)–(17) are brought into the Formula (18), respectively, and the gas flow equation of each component in the crack is obtained.

$$\phi_f\frac{\partial p_{fg}}{\partial t} + p_{fg}\frac{\partial \phi_f}{\partial t} + \nabla\left(\frac{k_f}{\mu}p_{fg}\nabla\left(p_{fg}+p_{fa}\right)\right) = \frac{V_m}{\tau\rho_c RT}\cdot\frac{\left(1-\phi_f\right)\left(p_m-p_{fg}\right)}{\left(\frac{V_L p_L}{(p_m+P_L)^2}+\frac{\phi_m}{\rho_c p_0}\right)} \tag{22}$$

$$\phi_f\frac{\partial p_{fa}}{\partial t} + p_{fa}\frac{\partial \phi_f}{\partial t} + \nabla\left(\frac{k_f}{\mu}p_{fa}\nabla\left(p_{fg}+p_{fa}\right)\right) = 0 \tag{23}$$

2.2.3. Evolution Law of Fracture Porosity and Permeability

According to the definition and geometric model, the porosity of the fracture system can be expressed as presented in reference [36].

$$\phi_f = \frac{\left(L_f+L_m\right)^3 - {L_m}^3}{\left(L_f+L_m\right)^3} \cong \frac{3L_f}{L_m} \tag{24}$$

Assuming that the deformation of coal body is elastic, and the deformation of coal matrix is much less than that of coal fracture system, which can be ignored, there are the following:

$$\frac{\phi_f}{\phi_{f0}} = \frac{L_f}{L_{f0}}\cdot\frac{L_{m0}}{L_m} \cong 1+\frac{\Delta L_f}{L_{f0}} = 1+\Delta\varepsilon_f, \tag{25}$$

where ϕ_f is the porosity of coal fracture system; L_m is the length of coal matrix; L_f is the crack width; L_{m0} is the initial length of coal matrix; L_{f0} is the crack width; and $\Delta\varepsilon_f$ is the volume strain of the fracture system.

Considering the movement of air components, the effective stress change in the cracks of the coal can be expressed as follows, based on the mechanical analysis of the coal:

$$\Delta\sigma^e = \sigma-\sigma_0-\left[\alpha_f\left(p_{fa}-p_{fa0}+p_{fg}-p_{fg0}\right)+\alpha_m\left(p_{mg}-p_{mg0}\right)\right], \tag{26}$$

where $\Delta\sigma^e$ is the variation of effective stress in coal; σ is the stress acting on coal; and σ_0 is the initial stress acting on coal.

The volumetric strain of the coal fracture system can be expressed as the sum of the strain resulting from matrix adsorption and the strain induced by effective stress in the fracture system, as follows:

$$\varepsilon_f = \varepsilon_s - \frac{\Delta\sigma^e}{K_f} = -\varepsilon_L\left(\frac{p_m}{p_L+p_m}-\frac{p_{m0}}{p_L+p_{m0}}\right) - \frac{1}{K_f}\left\{(\sigma-\sigma_0)-\left[\alpha_f\left(p_{fa}-p_{fa0}+p_{fg}-p_{fg0}\right)+\alpha_m\left(p_{mg}-p_{mg0}\right)\right]\right\} \tag{27}$$

$$K_f = L_f K_n. \tag{28}$$

The stress changes of the fracture system are as follows:

$$\Delta\sigma_f = -K_f\varepsilon_L\left(\frac{p_m}{p_L+p_m} - \frac{p_{m0}}{p_L+p_{m0}}\right) - \left\{(\sigma-\sigma_0) - \left[\alpha_f\left(p_{fa}-p_{fa0}+p_{fg}-p_{fg0}\right)+\alpha_m\left(p_{mg}-p_{mg0}\right)\right]\right\}, \tag{29}$$

where ε_f is the strain of coal mass fracture system; $\Delta\sigma_f$ is the stress variation of coal fracture system; ε_s is the adsorption strain caused by coal matrix; K_f is the equivalent bulk modulus of fracture; and K_n is the fracture stiffness.

The Formula (24) can be obtained in the substitution (22):

$$\frac{\phi_f}{\phi_{f0}} = 1+\Delta\varepsilon_f = 1-\varepsilon_L\left(\frac{p_m}{p_L+p_m} - \frac{p_{m0}}{p_L+p_{m0}}\right) - \frac{1}{K_f}\left\{(\sigma-\sigma_0) - \left[\alpha_f\left(p_{fa}-p_{fa0}+p_{fg}-p_{fg0}\right)+\alpha_m\left(p_{mg}-p_{mg0}\right)\right]\right\}. \tag{30}$$

Previous research has demonstrated a cubic relationship between coal permeability and coal porosity.

$$\frac{k_f}{k_{f0}} = \left(\frac{\phi_f}{\phi_{f0}}\right)^3 = \left\{1-\varepsilon_L\left(\frac{p_m}{p_L+p_m} - \frac{p_{m0}}{p_L+p_{m0}}\right) - \frac{1}{K_f}\left\{(\sigma-\sigma_0) - \left[\alpha_f\left(p_{fa}-p_{fa0}+p_{fg}-p_{fg0}\right)+\alpha_m\left(p_{mg}-p_{mg0}\right)\right]\right\}\right\}^3 \tag{31}$$

Figure 3 illustrates the governing equations and cross-coupling relationships of each physical field.

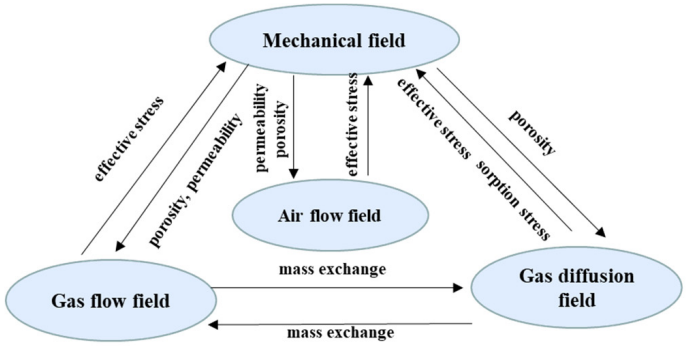

Deformation $Gu_{i,ij} + \frac{G}{1-2v}u_{j,ji} - \alpha_f\left(p_{fg,i}+p_{fa,i}\right) - \alpha_m p_{m,i} - K\varepsilon^s{}_{b,i}\delta_{ij} + F_i = 0$

Diffusion $\frac{\partial p_m}{\partial t} = -\frac{V_m}{\tau\rho_c RT}\cdot\frac{\left(p_m-p_{fg}\right)}{\left(\frac{V_L p_L}{(p_m+P_L)^2}+\frac{\phi_m}{\rho_c p_0}\right)}$

Gas flow $\phi_f\frac{\partial p_{fg}}{\partial t} + p_{fg}\frac{\partial\phi_f}{\partial t} + \nabla\left(\frac{k_f}{\mu}p_{fg}\nabla\left(p_{fg}+p_{fa}\right)\right) = \frac{V_m}{\tau\rho_c RT}\cdot\frac{\left(1-\phi_f\right)\left(p_m-p_{fg}\right)}{\left(\frac{V_L p_L}{(p_m+P_L)^2}+\frac{\phi_m}{\rho_c p_0}\right)}$

Air flow $\phi_f\frac{\partial p_{fa}}{\partial t} + p_{fa}\frac{\partial\phi_f}{\partial t} + \nabla\left(\frac{k_f}{\mu}p_{fa}\nabla\left(p_{fg}+p_{fa}\right)\right) = 0$

Fracture porosity $\frac{\phi_f}{\phi_{f0}} = 1+\Delta\varepsilon_f = 1-\varepsilon_L\left(\frac{p_m}{p_L+p_m} - \frac{p_{m0}}{p_L+p_{m0}}\right) - \frac{1}{K_f}\left\{(\sigma-\sigma_0) - \left[\alpha_f\left(p_{fa}-p_{fa0}+p_{fg}-p_{fg0}\right)+\alpha_m\left(p_{mg}-p_{mg0}\right)\right]\right\}$

Permeability $\frac{k_f}{k_{f0}} = \left(\frac{\phi_f}{\phi_{f0}}\right)^3 = \left\{1-\varepsilon_L\left(\frac{p_m}{p_L+p_m} - \frac{p_{m0}}{p_L+p_{m0}}\right) - \frac{1}{K_f}\left\{(\sigma-\sigma_0) - \left[\alpha_f\left(p_{fa}-p_{fa0}+p_{fg}-p_{fg0}\right)+\alpha_m\left(p_{mg}-p_{mg0}\right)\right]\right\}\right\}^3$

Figure 3. Governing equations and cross-coupling relations of each physical field.

3. Physical Model Establishment and Simulation Analysis

Using the constructed gas–air mixed flow model, numerical simulations were conducted to analyze the impact of extraction time, various negative pressures, and air leakage on gas concentration. The simulations also provided insights into the air leakage mechanism around the gas extraction borehole.

3.1. General Situation of Mine

Liuzhuang Coal Mine is situated in the western part of the Huainan coalfield and falls within the administrative jurisdiction of Yingshang County, Anhui Province. The mine's geographical coordinates range from approximately 116°07′30″ to 116°20′40″ east longitude and 32°45′00″ to 32°51′15″ north latitude. The mine field extends longitudinally for about 16 km from east to west and has a north–south width ranging from 3.5 to 8 km. The total area of the mine is approximately 82.2114 square kilometers, and the mining depth reaches −350 million meters. Within the Liuzhuang Coal Mine, several coal seams are identified as primary minable coal seams, namely, 13-1, 11-2, 8, 5, and 1. These seams have an average total thickness of 18.51 m. Additionally, there are several local minable coal seams, namely, 17-1, 16-1, 11-1, 9, 7-2, 6-1, 5-1, and 4, with a combined average total thickness of 9.07 m.

3.2. Physical Model

In this study, the numerical solution for the multi-field coupled seepage model is implemented using Comsol Multiphysics numerical simulation software 5.6, utilizing its built-in PDE module. The software employs a custom ultra-fine meshing method, resulting in a total of 6804 grids.

A gas drainage model is established for underground drilling at Liuzhuang Coal Mine, taking into account the geological, gas, and site conditions (as shown in Figure 4). The model has dimensions of 50 m (length) × 11 m (width), with a coal seam thickness of 3.10 m and an extraction hole diameter of 94 mm. It incorporates both mechanical and flow field boundaries. Regarding the mechanical boundary, the top of the model experiences a load boundary, representing an overlying strata pressure of 16 MPa, corresponding to a burial depth of 620 m. The left and right sides of the model have roller support boundaries with constrained normal displacement, while the bottom is fixed. As for the flow field boundary, which includes the matrix diffusion field and fracture seepage field, the initial gas pressure of the coal seam is set at 0.42 MPa. The boundary surrounding the coal seam and the sealing section of the borehole (16 m in length) are set with zero flow conditions. The effective drainage section of the borehole (20 m in length) is set to a negative pressure of 0.080 MPa (equivalent to a negative pressure of 15 kPa). Coal seam gas is naturally discharged from the coal wall of the roadway, with the boundary set at atmospheric pressure of 0.1 MPa. Table 1 provides the key parameters used as input for the model.

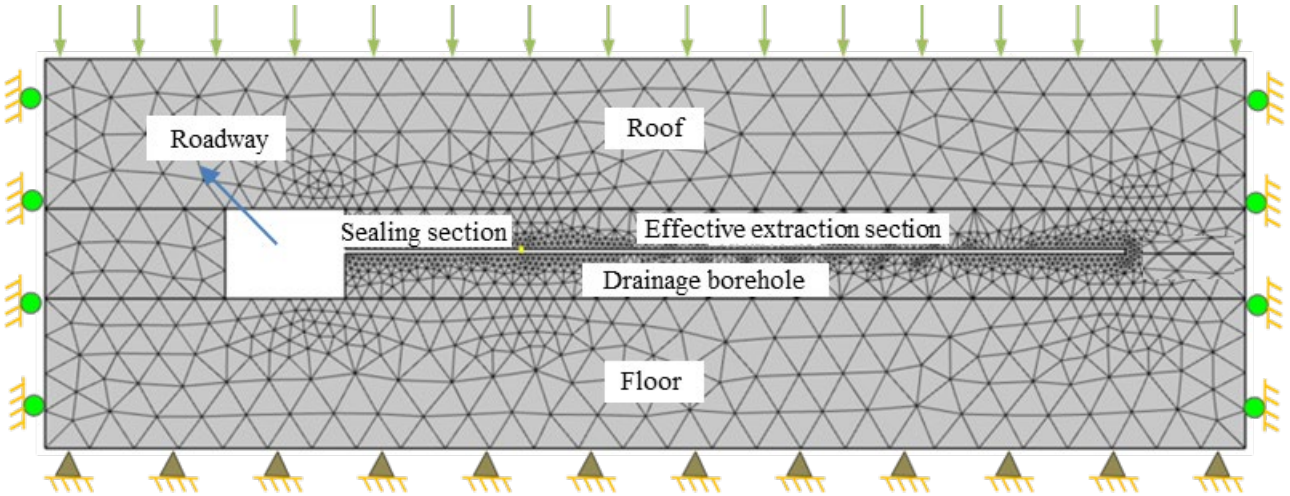

Figure 4. Gas drainage model by borehole.

Table 1. Parameters of multi-field coupling model.

Parameter	Value	Parameter	Value
Langmuir pressure constant (p_L)	6.019 (MPa)	Poisson's ratio of coal (ν_b)	0.3369
Molar volume (V_m)	16(m^3/mol)	Young's modulus of coal (E_b)	2843 (MPa)
Langmuir volume constant (V_L)	0.024 (m^3/kg)	Young's modulus of the coal grains (E_m)	8139 (MPa)
Langmuir volumetric strain constant (ε_L)	0.1726 (%)	Gas dynamic viscosity (μ)	1.08×10^{-5} (Pa·s)
Internal swelling ratio (F)	0.2	Density of coal (ρ_c)	1390 (kg/m^3)
Initial cohesion of coal (c)	1.6 (MPa)	Internal friction angle of coal (φ)	22 (°)
Coal temperature (T)	303.15 (K)	Molar gas constant(R)	8.314 (J/(mol·k))
Initial porosity of the matrix (ϕ_{m0})	0.06	Molar mass of gas (M_c)	0.016 (kg/mol)
Coal matrix adsorption time (τ)	13.66 (d)	Initial residual plastic strain (γ^{p*})	0.3326 (%)
Initial permeability of the matrix k_{f0}	0.05 (mD)	Initial fracture rate of coal (ϕ_{f0})	0.012

3.3. Permeability Distribution Law

Parallel to 1 m above the borehole, the distribution of coal seam permeability is as follows.

Figure 5 illustrates the distinctive characteristics of coal seam permeability along the depth of the borehole, dividing it into three zones: the pressure relief area, stress concentration area, and original stress area. When the borehole is in close proximity to the coal wall, the stress exerted on the coal body exceeds its yield limit, leading to the formation of fractures and a significant increase in permeability. This increased permeability creates pathways for air leakage, resulting in a decrease in gas concentration in this region. Without proper sealing measures, the gas concentration will continue to decrease. As the distance from the borehole increases, stress concentration occurs. In the stress concentration area, the permeability of the coal decreases, which leads to reduced gas fluidity and a decrease in the volume of gas extraction. When the coal body is located at a distance from the roadway and remains unaffected by driving and mining activities, its permeability maintains its original state. In this original stress area, the gas extraction volume stabilizes at a certain value.

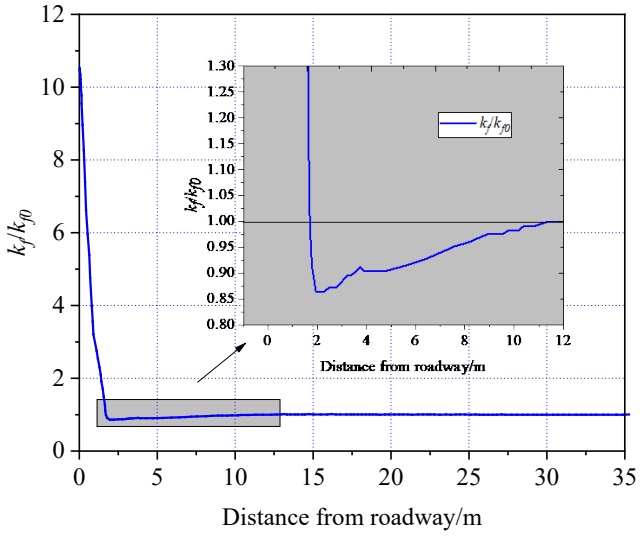

Figure 5. The change law of permeability along the depth of boreholes.

3.4. Analysis of the Influence of Negative Pressure on Gas Drainage

The application of negative pressure in gas drainage is aimed at facilitating the flow of free gas from fractures into boreholes. Once the fracture gas is expelled, a pressure difference is created between the gas in the matrix and the gas in the fractures. This pressure difference enables effective gas drainage. Theoretical Equations (19) and (20) suggest that in theory, increasing the negative pressure in drainage should weaken the flow of gas by reducing the pressure gradient of the fracture gas. In this study, a control variable

approach is utilized to simulate the occurrence of coal seam gas and borehole drainage under different negative pressure conditions while keeping other parameters constant. The simulation includes borehole gas flow, air leakage, and gas concentration. By analyzing the results, the relationship between borehole negative pressure and gas drainage is revealed. This research provides a theoretical basis for intelligently controlling the negative pressure in boreholes during the later stages of gas drainage.

3.4.1. Analysis of Gas Occurrence Law in Coal Seam under Different Negative Pressure

The simulation results demonstrate that the distribution of gas migration around the borehole follows a consistent trend across different borehole negative pressures (13 kPa, 15 kPa, 17 kPa, and 20 kPa). Therefore, Figure 6 displays the gas–air migration distribution specifically under a negative pressure of 15 kPa.

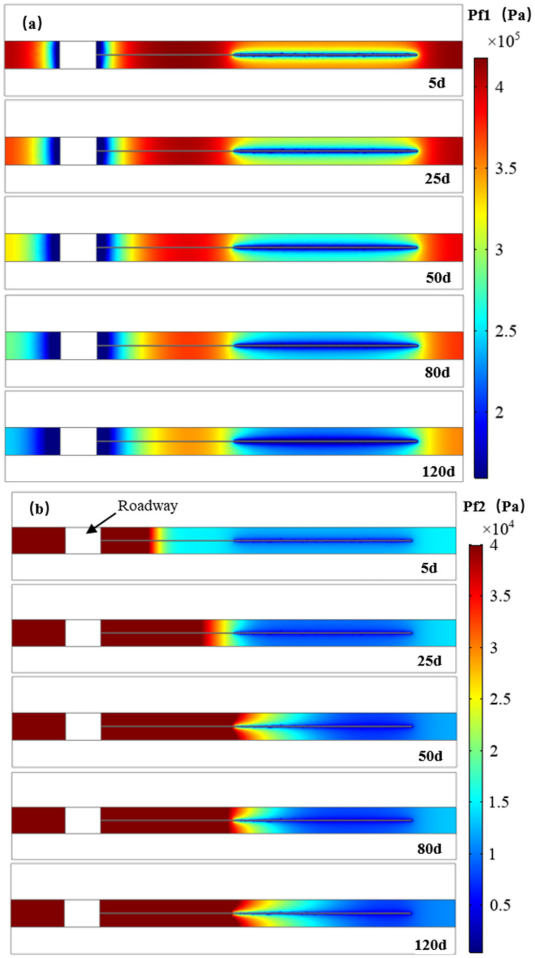

Figure 6. Gas distribution and migration in coal seam fissures around boreholes under the condition of 15 kPa negative pressure: (**a**) gas migration; (**b**) air migration.

In Figure 6, it is observed that the coal wall adjacent to the roadway, affected by mining disturbances, exhibits lower gas pressure compared to the extension of the boreholes where the gas pressure increases. This pressure difference drives the gas to flow into the boreholes and roadways under negative drainage pressure. Simultaneously, air in the roadway is pushed through mining-induced fracture channels towards the coal seam and boreholes by pressure gradients. During the initial stage of borehole gas drainage, the coal seam fissures have a high gas content and pressure gradient. As a result, a substantial amount of gas rushes into the boreholes under the influence of negative pressure drainage. Consequently, during this period, the gas concentration in the extraction borehole is relatively high, and the flow rate is considerable. However, as the drainage time progresses, the gas content

and pressure gradient in the coal surrounding the borehole gradually decrease. Conversely, the air content and pressure gradient in the coal around the borehole increase, leading to a continuous influx of air into the borehole. As a result, the flow rate of pure gas decreases while the gas concentration in the extraction borehole continues to decrease.

3.4.2. Gas Extraction from Boreholes under Different Negative Pressure

Different negative pressures of extraction have an impact on the air leakage in the cracks surrounding the borehole. Figure 7 illustrates the borehole drainage, including borehole gas flow, air leakage, and gas concentration, under different borehole negative pressures (13 kPa, 15 kPa, 17 kPa, and 20 kPa). According to Figure 7a,b, increasing the negative pressure of the borehole leads to an increase in gas flow and its attenuation rate within the borehole, along with an increase in air leakage. This can be attributed to several factors. Firstly, as the extraction time progresses, the effectiveness of negative pressure gradually weakens. Larger negative pressures contribute less to gas extraction. Instead, the larger negative pressure is primarily utilized to extract the air rushing into the borehole from the cracks surrounding it, resulting in a gradual increase in air leakage. Secondly, due to the dynamic pressure disturbance from the extraction borehole and the coal matrix shrinkage, the cracks surrounding the borehole gradually develop, resulting in a decrease in air leakage resistance and an increase in air leakage. Therefore, increasing the negative pressure of the boreholes reduces the gas concentration within the boreholes. Consequently, selecting an appropriate negative pressure is crucial for ensuring the economic cost and effectiveness of the project. It involves finding a balance between gas extraction efficiency, air leakage control, and overall project feasibility.

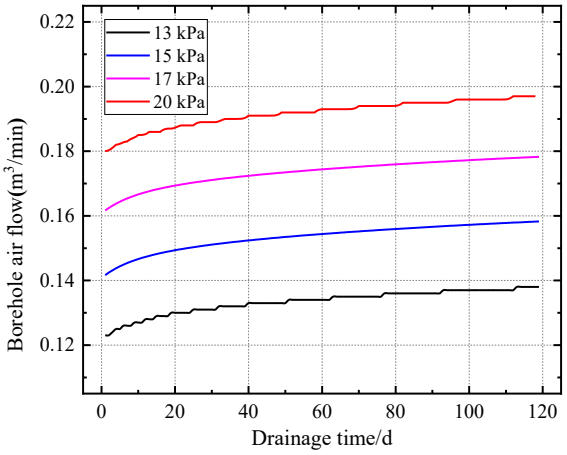

(**a**)

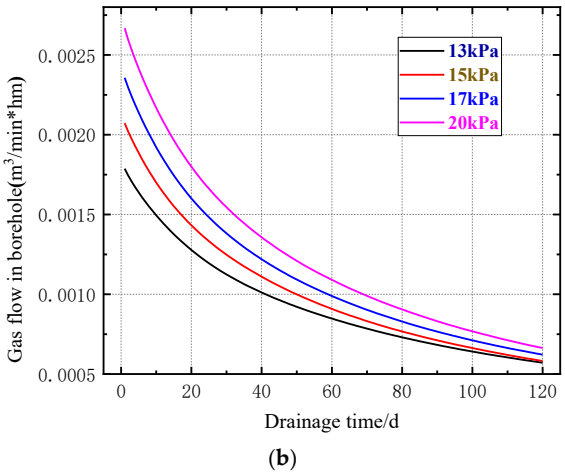

(**b**)

Figure 7. *Cont.*

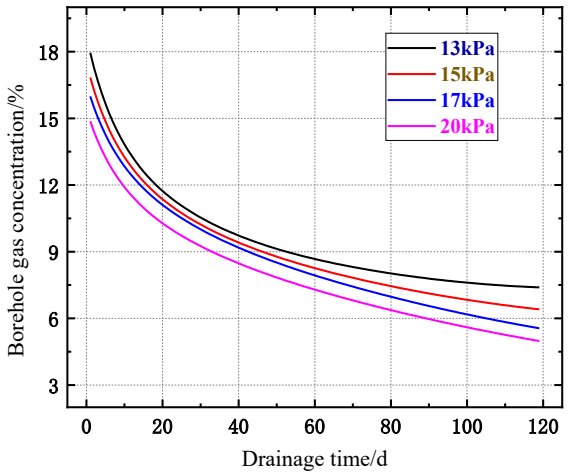

(**c**)

Figure 7. Gas drainage from boreholes with different negative pressure orders: (**a**) borehole air flow; (**b**) borehole gas flow; (**c**) gas concentration in boreholes.

3.4.3. Field Verification

According to the simulation results, the field test of 150804 is carried out to verify the accuracy of the model and provide the basis for regulation and control. The test scheme is as follows.

Figure 8 displays the specific drilling hole numbers along the groove, corresponding to the actual situation of the 150804 tape. The changes in flow rate and concentration negative pressure over time are investigated under different negative pressure conditions, namely, 13 kPa (No. 1), 15 kPa (No. 2), and 20 kPa (No. 3). The single holes are identified as No. 1–3 boreholes, while the group boreholes are labeled as No. 4–18. The group holes are further divided into three groups: 13 kPa (No. 4–8), 15 kPa (No. 9–13), and 20 kPa (No. 14–18). The specific connection mode among these boreholes is illustrated in Figure 8.

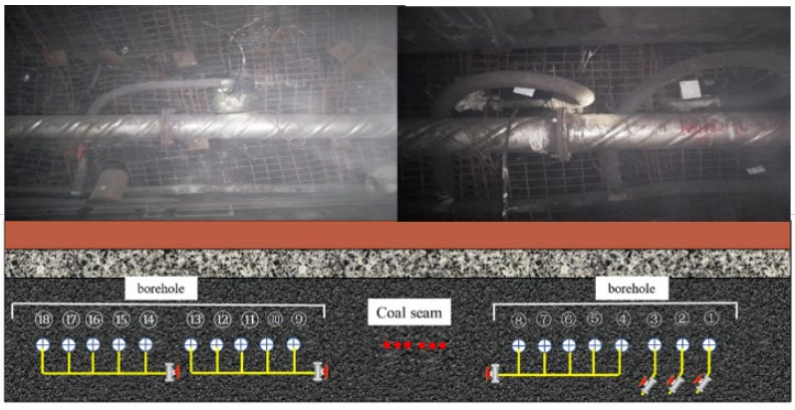

Figure 8. 150804 Test drilling scheme diagram.

Figure 9 illustrates a comparison between the field-measured concentration and flow data of hole 2 (15 kPa) and the corresponding simulated data. The results show that as the pumping time increases, the extraction concentration and flow rate of the test borehole exhibit a decreasing trend. Specifically, the extraction concentration decreases from 16% to approximately 5%, while the flow rate decreases from 0.002 m^3/min to 0.0005 m^3/min. Importantly, the field-measured data demonstrate a good agreement with the simulated data, with concentration and flow rate errors of less than 10%. This confirms the validity of the model and provides a solid basis for the regulation and control of gas drainage boreholes.

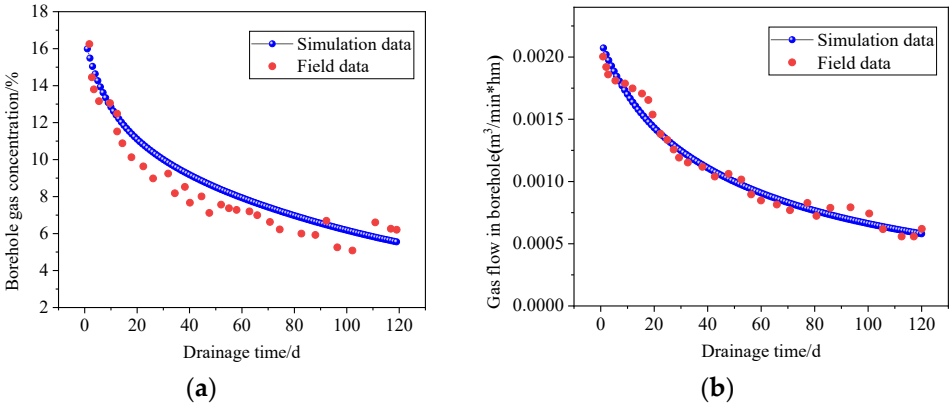

Figure 9. Comparison between field data and simulation data: (**a**) drill gas concentration decay curve over time; (**b**) drill flow decay curve over time.

3.4.4. Negative Pressure Control System

Figure 10 illustrates the architecture of the gas extraction control system, which consists of three main components: an intelligent integrated management and control platform, an underground monitoring and control substation, and a system communication transmission. The intelligent terminal includes a laser methane multi-parameter analyzer installed on the gas pumping pipelines at the test face, as well as an electric device for mine flameproof valves. These terminals are responsible for monitoring the extraction state parameters such as gas concentration, extraction negative pressure, flow rate, CO concentration, and temperature. They also adjust the valve opening state accordingly. The underground monitoring and control substation performs essential functions such as data storage, data transit, and direct control of terminal equipment. These functions are realized through the substation's PLC control cabinet. The communication transmission part facilitates the underground data upload, transit, and ground command issuance. The logic of this component is as follows: the underground monitoring and control substation accesses the mining industrial ring network through optical fiber; the relevant information is then transmitted back to the ground intelligent integrated management and control platform via a switch. Valve regulation can be effectively carried out on the ground platform.

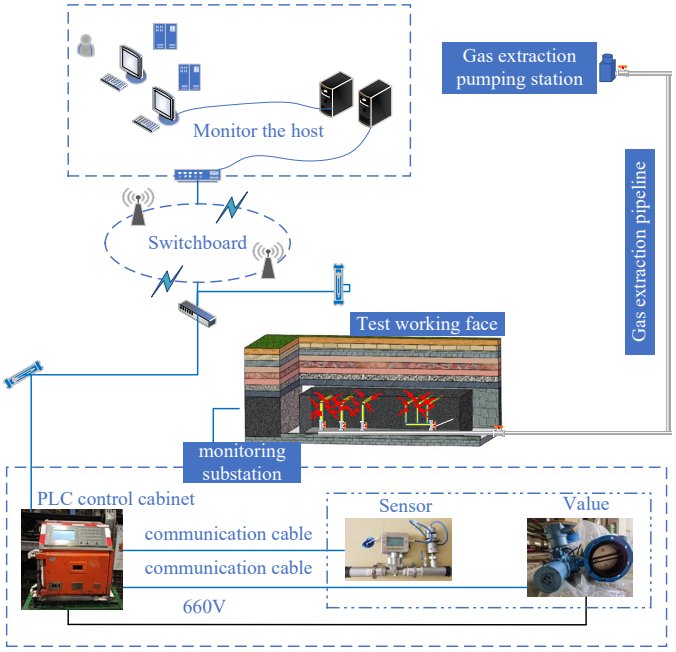

Figure 10. Gas negative pressure regulation system architecture.

In order to further validate the effectiveness of negative pressure control, a solenoid valve is installed for the purpose of opening, closing, and adjusting, as shown in Figure 11. Based on the research conclusions regarding the influence of negative pressure on gas extraction effectiveness, a negative pressure adjustment test was conducted on the extraction at the 150804 face of Liuzhuang Coal Mine. The results indicate that after pumping the test single hole, the initial gas concentration is approximately 40%. However, the gas concentration decreases rapidly over time. After implementing control measures, the concentration in the drilling hole increased by around 10%, representing a relative increase ratio of more than 40%. The higher concentration extraction was maintained for nearly 3 to 4 weeks, significantly improving the extraction effectiveness (Figure 12). Considering the fast attenuation rate of gas concentration in the working face and the short duration of high concentration extraction, the simulation results mentioned above suggest that the borehole gas concentration in the control group during the later stages of extraction is lower than that in the test hole. This discrepancy could be attributed to the increased air leakage resulting from the mining side's negative pressure setting being too high.

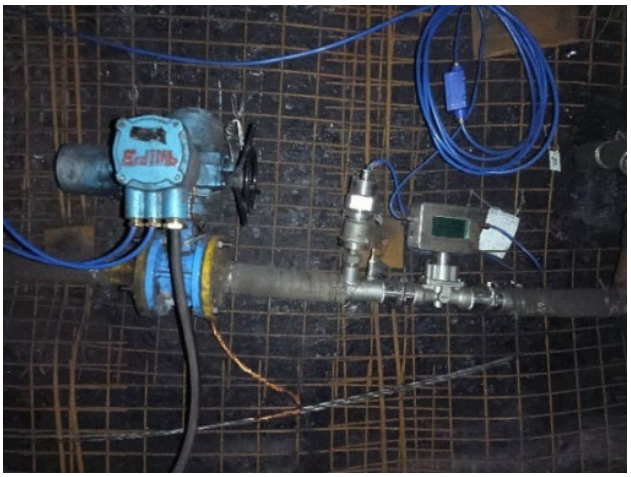

Figure 11. Installation drawing of solenoid valve.

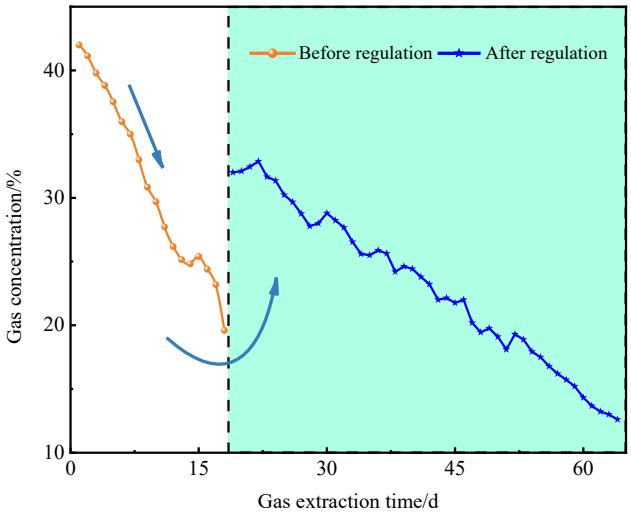

Figure 12. Drill control effect diagram.

Manual regulation of the negative pressure is carried out to assess its impact on gas drainage. By carefully regulating and controlling the negative pressure, the gas concentration in an individual borehole is maintained at a stable level exceeding 25%. Figure 13 illustrates this data, highlighting the improved extraction capacity of the mine and ensuring the safe production of the coal mine.

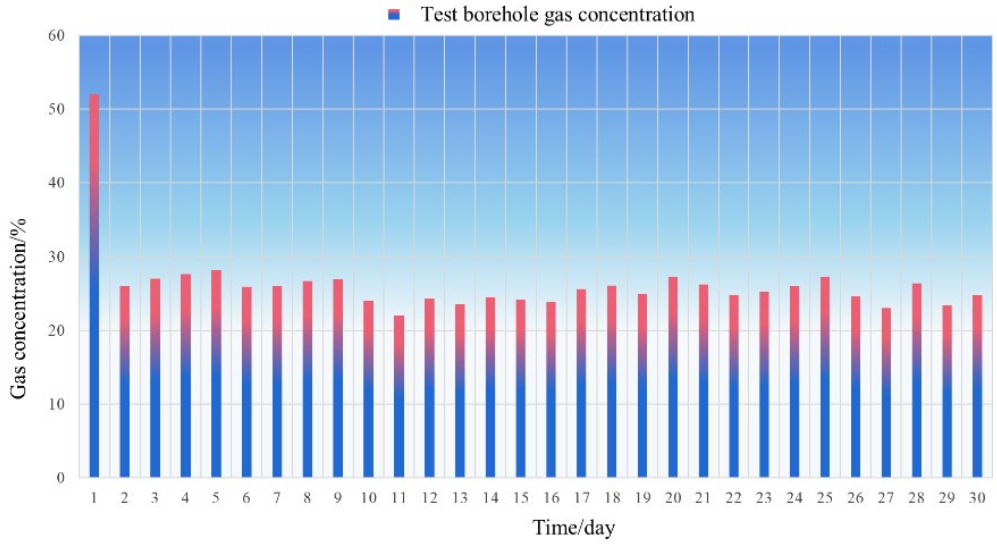

Figure 13. Gas concentration diagram of test borehole.

4. Conclusions

In this paper, we have successfully established an air leakage model for boreholes in coal mining. We have investigated the gas–air migration law and air leakage mechanism during gas drainage using this model and verified its accuracy. The main findings of our study are summarized as follows:

(1) In this study, we have incorporated the elastic–plastic mechanics theory of coal, Fick's law, and Darcy's law to derive the governing equation for coal deformation and the dynamic change equation for permeability. Building upon the double porosity medium model, we have developed a comprehensive coupling model for the "coal seam gas–air" binary mixed gas. This model takes into account crucial factors such as coal matrix deformation, pore gas diffusion, fracture gas seepage, and gas leakage. By considering these elements, our model provides a solid theoretical foundation for analyzing the impact of negative pressure on gas drainage effectiveness.

(2) In our research, we have conducted simulations to study the variations of gas flow and gas concentration over time under different negative pressure conditions. By comparing the simulation results with the field test data, we have found that our model exhibits good agreement with the actual measurements. This validation of our model provides a solid basis for regulating negative pressure in gas drainage operations.

(3) During the gas drainage process, the application of negative pressure plays a crucial role in facilitating the flow of free gas into the borehole. This creates a pressure difference between the matrix and the fractured gas, allowing for the effective drainage of gas. However, as the extraction time increases, the diminishing effect of negative pressure reduces its contribution to gas flow, leading to more significant air leakage. To address this issue, it is important to reduce the negative pressure during the later stages of gas extraction. By doing so, we can minimize air leakage, improve gas concentration, and enhance the utilization of resources.

(4) The collected data clearly indicate that the implementation of negative pressure control in gas drilling at the test face has resulted in a significant improvement in the gas concentration of the borehole. The gas concentration of the drainage gas is consistently maintained at levels exceeding 25%. This enhancement in gas concentration has led to a significant improvement in the extraction capacity, which effectively ensures the safety of mine production.

Author Contributions: Conceptualization, H.G. and F.D.; methodology, X.C.; software, H.G.; validation, J.Z., X.C. and A.Z.; formal analysis, H.G.; investigation, F.D.; resources, H.G.; data curation, F.D.; writing—original draft preparation, H.G.; writing—review and editing, H.G.; project administration, J.Z.; funding acquisition, F.D. All authors have read and agreed to the published version of the manuscript.

Funding: This research was funded by National Natural Science Foundation of China (No. 52130409, No. 52121003).

Data Availability Statement: The data are available from the corresponding author on reasonable request.

Acknowledgments: We would like to thank the anonymous reviewers for their valuable comments and suggestions that lead to a substantially improved manuscript.

Conflicts of Interest: The authors declare no conflict of interest.

References

1. Cai, Y.; Liu, D.; Pan, Z.; Yao, Y.; Li, J.; Qiu, Y. Pore structure and its impact on CH_4 adsorption capacity and flow capability of bituminous and subbituminous coals from Northeast China. *Fuel* **2013**, *103*, 258–268. [CrossRef]
2. Hao, Y.; Zhang, Z.; Liao, H.; Wei, Y. China's farewell to coal: A forecast of coal consumption through 2020. *Energy Pol.* **2015**, *86*, 444–455. [CrossRef]
3. Tang, X.; Wang, Z.; Ripepi, N.; Kang, B.; Yue, G. Adsorption affinity of different types of coal: Mean isosteric heat of adsorption. *Energy Fuels* **2015**, *29*, 3609–3615. [CrossRef]
4. Sun, L.; Wang, H.; Zhang, C.; Zhang, S.; Liu, N.; He, Z. Evolution of methane ad-/desorption and diffusion in coal under in the presence of oxygen and nitrogen after heat treatment. *J. Nat. Gas Sci. Eng.* **2021**, *95*, 104196. [CrossRef]
5. Aguado, M.; Nicieza, C. Control and prevention of gas outbursts in coal mines, Riosa–Olloniego coalfield, Spain. *Int. J. Coal Geol.* **2007**, *69*, 253–266. [CrossRef]
6. Beamish, B.; Crosdale, P. Instantaneous outbursts in underground coal mines: An overview and association with coal type. *Int. J. Coal Geol.* **1998**, *35*, 27–55. [CrossRef]
7. Black, D.J. Review of coal and gas outburst in Australian underground coal mines. *Int. J. Min. Sci. Technol.* **2019**, *29*, 815–824. [CrossRef]
8. Zhao, W.; Wang, K.; Cheng, Y. Evolution of gas transport pattern with the variation of coal particle size: Kinetic model and experiments. *Powder Technol.* **2020**, *367*, 336–346. [CrossRef]
9. Yuan, L. Theory of pressure-relieved gas extraction and technique system of integrated coal production and gas extraction. *J. China Coal Soc.* **2009**, *34*, 1–8.
10. Cheng, Y.; Fu, J.; Yu, Q. Development of Gas Extraction Technology in Coal Mines of China. *J. Min. Saf. Eng.* **2009**, *26*, 127–139.
11. Frank, H.; Ting, R.; Naj, A. Evolution and application of in-seam drilling for gas drainage. *Int. J. Min. Sci. Technol.* **2013**, *23*, 543–553. [CrossRef]
12. Hungerford, F.; Ren, T. Directional drilling in unstable environments. *Int. J. Min. Sci. Technol.* **2014**, *24*, 397–402. [CrossRef]
13. Aminossadati, S.; Amanzadeh, M.; Prochon, E. Step change approaches in coal technology and fugitive emissions research. *Int. J. Min. Sci. Technol.* **2014**, *24*, 363–367. [CrossRef]
14. Zhou, F.; Sun, Y.; Li, H.; Yu, G. Research on the theoretical model and engineering technology of the coal seam gas drainage hole sealing. *J. China Univ. Min. Technol.* **2016**, *45*, 433–439.
15. Wang, G.; Wang, K.; Jiang, Y. Reservoir Permeability Evolution during the Process of CO_2-Enhanced Coalbed Methane Recovery. *Energies* **2018**, *11*, 2996. [CrossRef]
16. Liu, T.; Lin, B.; Yang, W. Dynamic diffusion-based multifield coupling model for gas drainage. *J. Nat. Gas Sci. Eng.* **2017**, *44*, 233–249. [CrossRef]
17. Liu, J.; Chen, Z.; Elsworth, D. Interactions of multiple processes during CBM extraction: A critical review. *Int. J. Coal Geol.* **2011**, *87*, 175–189. [CrossRef]
18. Liang, B.; Yuan, X.; Sun, W. Seepage coupling model of in-seam gas extraction and its applications. *J. China Univ. Min. Technol.* **2014**, *2*, 208–213.
19. Wu, Y. Dual poroelastic response of coal to CO_2 sequestration. *J. China Coal Soc.* **2011**, *36*, 889–890.
20. Zhai, C.; Chen, Z.; Kizil, M. Characterisation of mechanics and flow fields around in-seam methane gas drainage borehole for preventing ventilation air leakage: A case study. *Int. J. Coal Geol.* **2016**, *162*, 123–138.
21. Cheng, Y.; Dong, J.; Li, W.; Chen, M.; Liu, K. Effect of negative pressure on coalbed methane extraction and application in the utilization of methane resource. *J. China Coal Soc.* **2017**, *42*, 1466–1473.
22. Hao, F.; Liu, Y.; Long, W.; Zuo, W. Effective gas extraction radius of different burial depths under creep-seepage coupling. *J. China Coal Soc.* **2017**, *42*, 130–136.
23. Wang, D.; Peng, M.; Fu, Q.; Qin, H.; Xia, Y. Evolution and numerical simulation of coal permeability during gas drainage in coal seams. *Chin. J. Rock Mech. Eng.* **2016**, *35*, 704–712.

24. Wang, K.; Liu, A.; Zhou, A. Theoretical analysis of influencing factors on resistance in the process of gas migration in coal seams. *Int. J. Min. Sci. Technol.* **2017**, *27*, 315–319. [CrossRef]
25. Zang, J.; Wang, K.; Liu, A.; Zhang, X.; Yan, Z. An orthotropic coal permeability model. *J. China Univ. Min. Technol.* **2019**, *4*, 36–45.
26. Liu, Q.; Cheng, Y.; Zhou, H. A mathematical model of coupled gas flow and coal deformation with gas diffusion and Klinkenberg effects. *Rock Mech. Rock Eng.* **2015**, *48*, 1163–1180. [CrossRef]
27. Liu, T.; Lin, B.; Yang, W. Impact of matrix–fracture interactions on coal permeability: Model development and analysis. *Fuel* **2017**, *207*, 522–532. [CrossRef]
28. Zhang, X.; Gao, J.; Jia, G.; Zhang, J. Study on the influence mechanism of air leakage on gas extraction in extraction boreholes. *Energy Explor. Exploit.* **2022**, *40*, 1344–1359. [CrossRef]
29. Liu, T.; Zhao, Y.; Kong, X.; Lin, B.; Zou, Q. Dynamics of coalbed methane emission from coal cores under various stress paths and its application in gas extraction in mining-disturbed coal seam. *J. Nat. Gas Sci. Eng.* **2022**, *104*, 104677. [CrossRef]
30. Zhang, N.; Li, X.; Cheng, H. A coupled damage-hydro-mechanical model for gas drainage in low-permeability coalbeds. *J. Nat. Gas Sci. Eng.* **2016**, *35*, 1032–1043. [CrossRef]
31. Guan, C.; Liu, S.; Li, C.; Wang, Y.; Zhao, Y. The temperature effect on the methane and CO_2 adsorption capacities of Illinois coal. *Fuel* **2018**, *211*, 241–250. [CrossRef]
32. Liu, T.; Lin, B.; Fu, X. Modeling air leakage around gas extraction boreholes in mining-disturbed coal seams. *Process Saf. Environ. Prot.* **2020**, *141*, 202–214. [CrossRef]
33. Wang, H.; Wang, E.; Li, Z. Study on sealing effect of pre-drainage gas borehole in coal seam based on air-gas mixed flow coupling model. *Process Saf. Environ. Prot.* **2020**, *136*, 15–27. [CrossRef]
34. Chen, M.; Cheng, Y.; Li, H.; Wang, L.; Jin, K.; Dong, J. Impact of inherent moisture on the methane adsorption characteristics of coals with various degrees of metamorphism. *J. Nat. Gas Sci. Eng.* **2018**, *55*, 312–320. [CrossRef]
35. Ji, H.; Li, Z.; Yang, Y.; Hu, S.; Peng, Y. Effects of organic micro molecules in coal on its pore structure and gas diffusion characteristics. *Transp. Porous Media* **2015**, *107*, 419–433. [CrossRef]
36. Liu, T.; Lin, B.; Fu, X. Modeling coupled gas flow and geomechanics process in stimulated coal seam by hydraulic flushing. *Int. J. Rock Mech. Min. Sci.* **2021**, *142*, 104769. [CrossRef]